ORIGINAL PAPER

First evaluation of stiff-in-soft host–inclusion systems: experimental synthesis of zircon inclusions in quartz crystals

Joseph P. Gonzalez[1,5] · Jay B. Thomas[2] · Mattia L. Mazzucchelli[3,6] · Ross J. Angel[4] · Matteo Alvaro[1]

Abstract

Quartz crystals with zircon inclusions were synthesized using a piston-cylinder apparatus to experimentally evaluate the use of inclusions in "soft" host minerals for elastic thermobarometry. Synthesized zircon inclusion strains and, therefore, pressures (P_{inc}) were measured using Raman spectroscopy and then compared with the expected inclusion strains and pressures calculated from elastic models. Measured inclusion strains and inclusion pressures are systematically more tensile than the expected values and, thus, re-calculated entrapment pressures are overestimated. These discrepancies are not caused by analytical biases or assumptions in the elastic models and strain calculations. Analysis shows that inclusion strain discrepancies progressively decrease with decreasing experimental temperature in the α-quartz field. This behavior is consistent with inelastic deformation of the host–inclusion pairs induced by the development of large differential stresses during experimental cooling. Therefore, inclusion strains are more reliable for inclusions trapped at lower temperature conditions in the α-quartz field where there is less inelastic deformation of the host–inclusion systems. On the other hand, entrapment isomekes of zircon inclusions entrapped in the β-quartz stability field plot along the α–β quartz phase boundary, suggesting that the inclusion strains were mechanically reset at the phase boundary during experimental cooling and decompression. Therefore, inclusions contained in soft host minerals can be used for elastic thermobarometry and inclusions contained in β-quartz may provide constraints on the P–T at which the host–inclusion system crossed the phase boundary during exhumation.

Keywords Quartz · Zircon · Host-inclusion · Elastic thermobarometry · Piston-cylinder

✉ Joseph P. Gonzalez
  joseph.gonzalez@unipv.it

1 Department of Earth and Environmental Sciences, University of Pavia, Pavia, Italy

2 Department of Earth and Environmental Sciences, Syracuse University, Syracuse, NY, USA
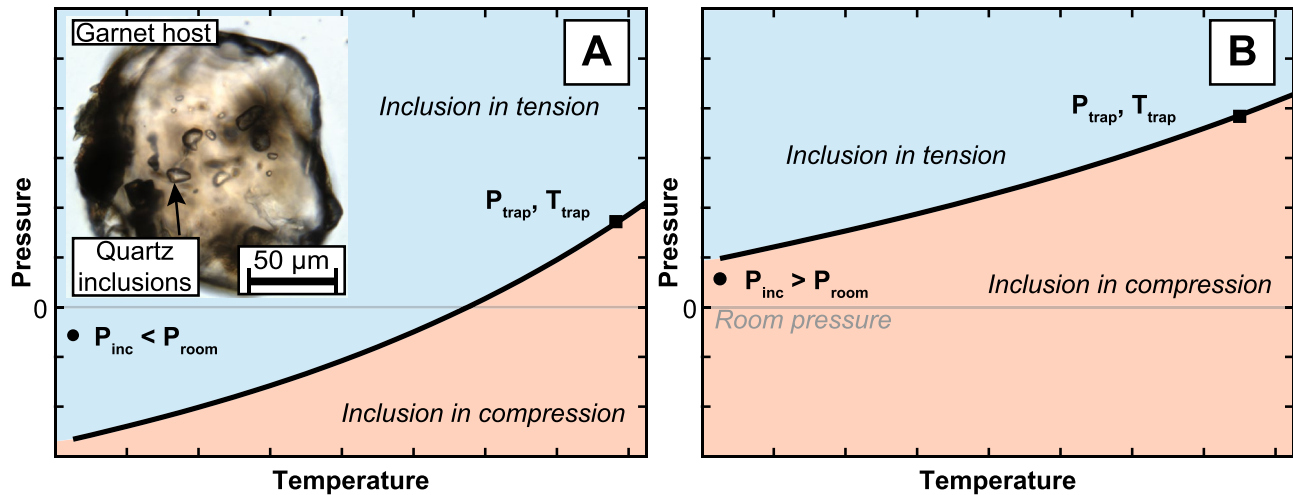
3 Mainz Institute of Multiscale Modeling and Institute of Geoscience, Johannes-Gutenberg University of Mainz, Mainz, Germany
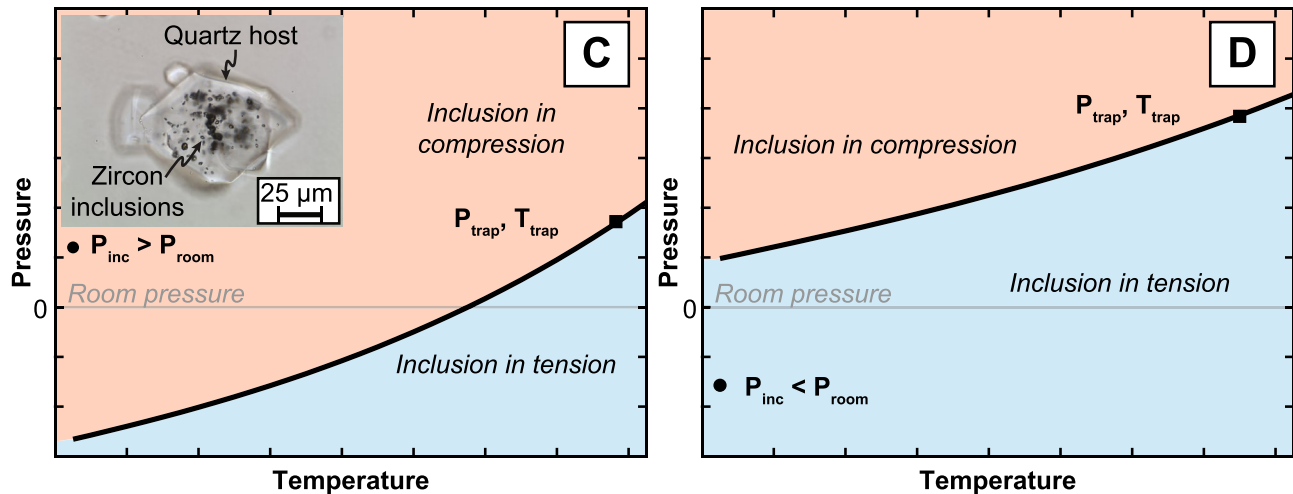
4 IGG-CNR, Padua, Italy

5 Present Address: Department of Geosciences, University of Wisconsin-Madison, Madison, WI, USA

6 Present Address: Institute of Earth Sciences, University of Lausanne, Lausanne, Switzerland

Introduction

Elastic models can be applied to host–inclusion systems in rocks and used for thermobarometry when there is a contrast between the elastic properties of the host and inclusion minerals (e.g., Angel et al. 2014; Kohn et al. 2023). Host–inclusion systems have been frequently used to constrain the P–T conditions of elastic equilibration during metamorphism of relatively soft inclusions contained in comparatively stiff host minerals (e.g., Gonzalez et al. 2019; Gilio et al. 2021; Baldwin et al. 2021). However, stiff inclusions entrapped in soft hosts are rarely used for elastic thermobarometry despite the fact that, if the host–inclusion system is behaving elastically, these host–inclusion systems should yield similar P–T constraints (Fig. 1; Kohn 2014; Angel et al. 2015).

Quartz is often used for elastic thermobarometry because its elastic properties and behavior across the α–β phase boundary are well constrained (e.g., Angel et al. 2017a), and it is commonly preserved as inclusions in other minerals. Moreover, quartz is also a major rock forming

Soft inclusion in stiff host mineral

A Garnet host — Quartz inclusions — 50 μm
Inclusion in tension
P_{trap}, T_{trap}
Pressure
0
● $P_{inc} < P_{room}$
Inclusion in compression
Temperature

B
Inclusion in tension
P_{trap}, T_{trap}
Pressure
0
● $P_{inc} > P_{room}$
Inclusion in compression
Room pressure
Temperature

Stiff inclusion in soft host mineral

C Quartz host — Zircon inclusions — 25 μm
Inclusion in compression
P_{trap}, T_{trap}
Pressure
● $P_{inc} > P_{room}$
Room pressure
0
Inclusion in tension
Temperature

D
Inclusion in compression
P_{trap}, T_{trap}
Pressure
0
Room pressure
Inclusion in tension
● $P_{inc} < P_{room}$
Temperature

Fig. 1 Schematic diagrams of the stress state of an inclusion entrapped in a host mineral at various *P–T* conditions. **A** and **B** show the behavior of a soft inclusion in a stiff host mineral such as a quartz inclusion in a garnet host (inset image modified from Gonzalez et al. 2019), and **C** and **D** show the behavior of a stiff inclusion in a soft host such as a zircon inclusion in a quartz host

mineral that (re)crystallizes in a variety of geologic settings and often entraps stiffer mineral inclusions, such as zircon. Until recently, the use of quartz as a host mineral was also limited because elastic models were strictly applicable to mineral inclusions contained in elastically isotropic host minerals (Zhang 1998; Guiraud and Powell 2006; Angel et al. 2017b). This limitation excluded the use of quartz as a host for elastic thermobarometry because of its well-known elastic anisotropy (e.g., Lakshtanov et al. 2007). However, a new elastic model was developed that accounts for the elastic interactions in fully anisotropic host–inclusion systems (Gonzalez et al. 2021) and can now be used to evaluate the elastic deformation between stiff zircon inclusions in quartz hosts that were experimentally synthesized over a range of *P–T* conditions.

To evaluate the use of stiff inclusions contained in quartz for elastic thermobarometry, we used a piston–cylinder apparatus to synthesize zircon inclusions in quartz (ZiQ) over a range of pressure and temperature conditions. We then used the anisotropic elastic model (Gonzalez et al. 2021) to evaluate the expected elastic behavior of the inclusions for the given experimental conditions. Then, Raman shifts measured from the experimentally crystallized inclusions were used to determine the strains and remnant pressures (P_{inc}) for comparison with the model calculations. Entrapment conditions were then re-calculated from the measured P_{inc} values for comparison with the experimental conditions.

Methods

Piston-cylinder experiments

Ten experiments were performed at various *P–T* conditions using an end-loaded piston-cylinder apparatus (Fig. S1; Boyd and England 1960). Oxides were used as starting materials (Alfa Aesar amorphous SiO_2, Alfa Aesar ZrO_2, and water). Runs to simultaneously synthesize quartz and zircon were made at pressures ranging from 0.8 to 2.5 GPa

and temperatures ranging from 700 to 900 °C (full details in Supplemental Materials). Each experiment was run at the target *P–T* condition for a period of 72 h and then quenched to below 100 °C within 20 s by turning off the furnace power. During the experimental quench the pressure drops by approximately 30% of the experimental pressure condition. Pressure on the experimental assembly was then slowly released. The exact *P–T* paths during ramp-up and take-down of the experiment varied depending on the targeted *P–T* conditions, but are similar to that shown in
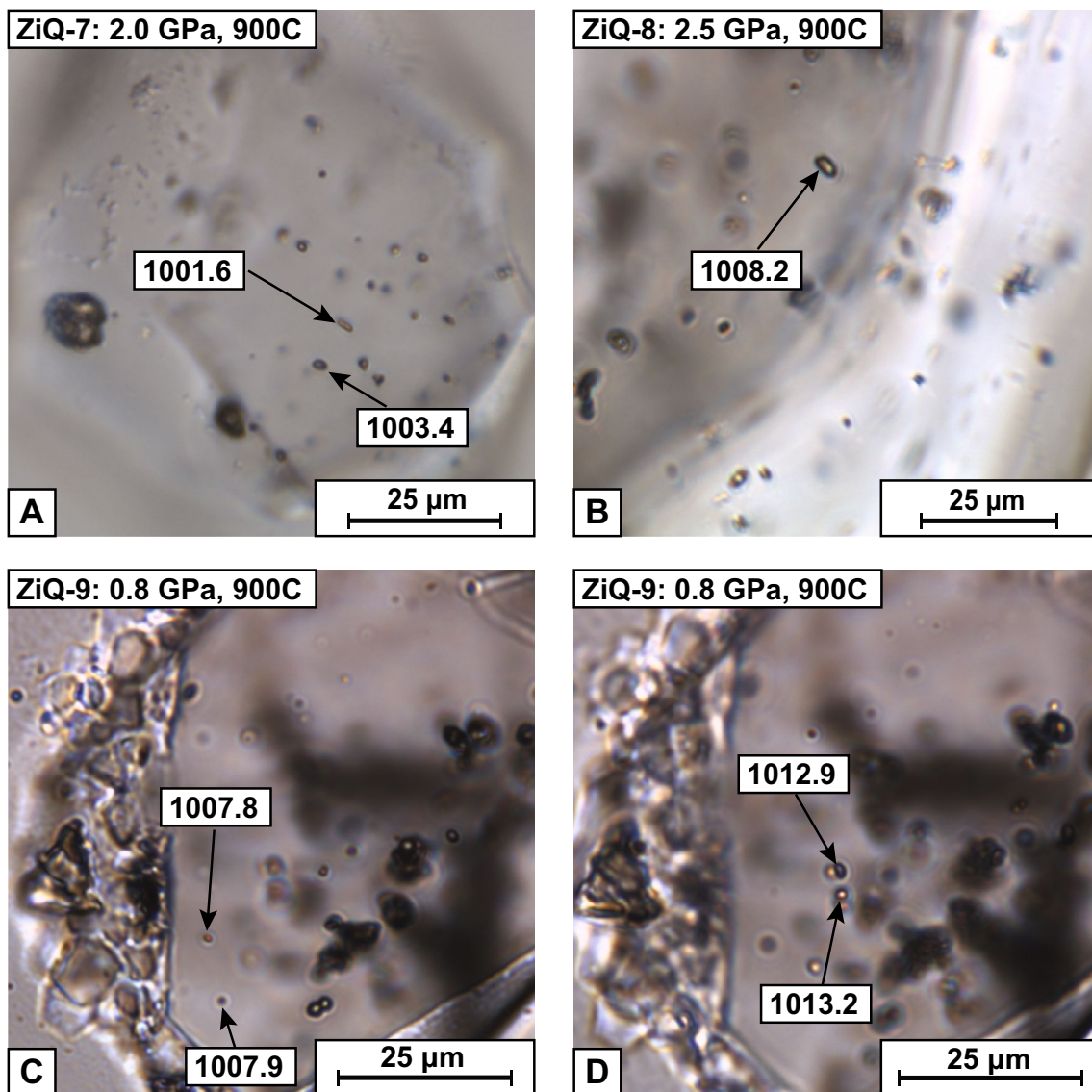
Fig. 2 Transmitted light photomicrographs of synthesized zircon inclusions showing the effects of inclusion geometry and elastic isolation on the position of the 1008 cm^{-1} peak of zircon. **A** Photomicrograph showing the effect of inclusion geometry on the Raman peak position. **B** Zircon inclusions in quartz crystallized in experiment ZiQ-8 at 2.5 GPa, 900 °C with Raman peak positions that correspond to ambient *P–T* conditions. **C** Photomicrographs of two inclusions located near the surface of the polished quartz crystal that yield Raman peak positions that correspond to ambient conditions. **D** Two inclusions located deeper in the same host quartz crystal in **C** but are located in < 5 inclusion radii proximity and give large shifts

Thomas and Spear (2018). Quartz and zircon were the only minerals crystallized in the experiments (Fig. 2).

Host–inclusion elastic thermobarometry calculations

Elastically isolated zircon inclusions in quartz were measured using confocal Raman spectroscopy (see Supplemental Materials for details). Measured Raman shifts of the zircon 1008, 975, 438, 356, 224, 213, and 201 cm^{-1} bands and the phonon-mode Grüneisen tensor of zircon (Stangarone et al. 2019) were used in stRAinMAN (Angel et al. 2019) to calculate the strains within the inclusions. Application of the phonon-mode Grüneisen tensor of zircon assumes that the inclusion symmetry is not broken and the constraints of tetragonal symmetry are still valid. Therefore, in our calculations, we obtain the residual strains as $\varepsilon_1 = \varepsilon_2 \neq \varepsilon_3$, which may be different from the real residual strains where $\varepsilon_1 \neq \varepsilon_2$ and the components ε_4, ε_5, and ε_6 can be non-zero and depend on the relative crystallographic orientation (RCO; Gonzalez et al. 2021). Strains were then used in conjunction with the room-temperature elastic tensor of zircon (Özkan et al. 1974) to calculate the remnant stresses. The remnant

pressure (P_{inc}) in the inclusion was then calculated as the average of the three normal stresses.

Multiple combinations of Raman bands were also tested to ensure consistency, including the exclusion of the 201, 213, 224 cm^{-1} bands (which are highly dependent on Zr and are less sensitive to strain; Stangarone et al. 2019), and all various combinations of at least three of the remaining four Raman bands (i.e., the 356, 438, 975, 1008 cm^{-1} bands; Fig. 3). Multiple inclusions from each experiment where all Raman bands were measured were selected for strain calculation tests. Results from these calculations show that the calculated strains from all combinations are generally indistinguishable within errors, and only the combination that excluded the 975 cm^{-1} band occasionally yielded different strain results (Fig. 3A–C). Despite this, the P_{inc} from the strains of all Raman band combinations are the same within the uncertainties (Fig. 3D–F). Therefore, we chose to use all the Raman bands in our strain calculations because this reduced the uncertainty on the strains.

Entrapment conditions of the synthesized inclusions were then calculated for comparison with the experimental P–T conditions using the isotropic elastic model of Angel et al. (2017b), the volume EoS of quartz (Angel et al. 2017a) and zircon (Ehlers et al. 2022), and the measured P_{inc} values
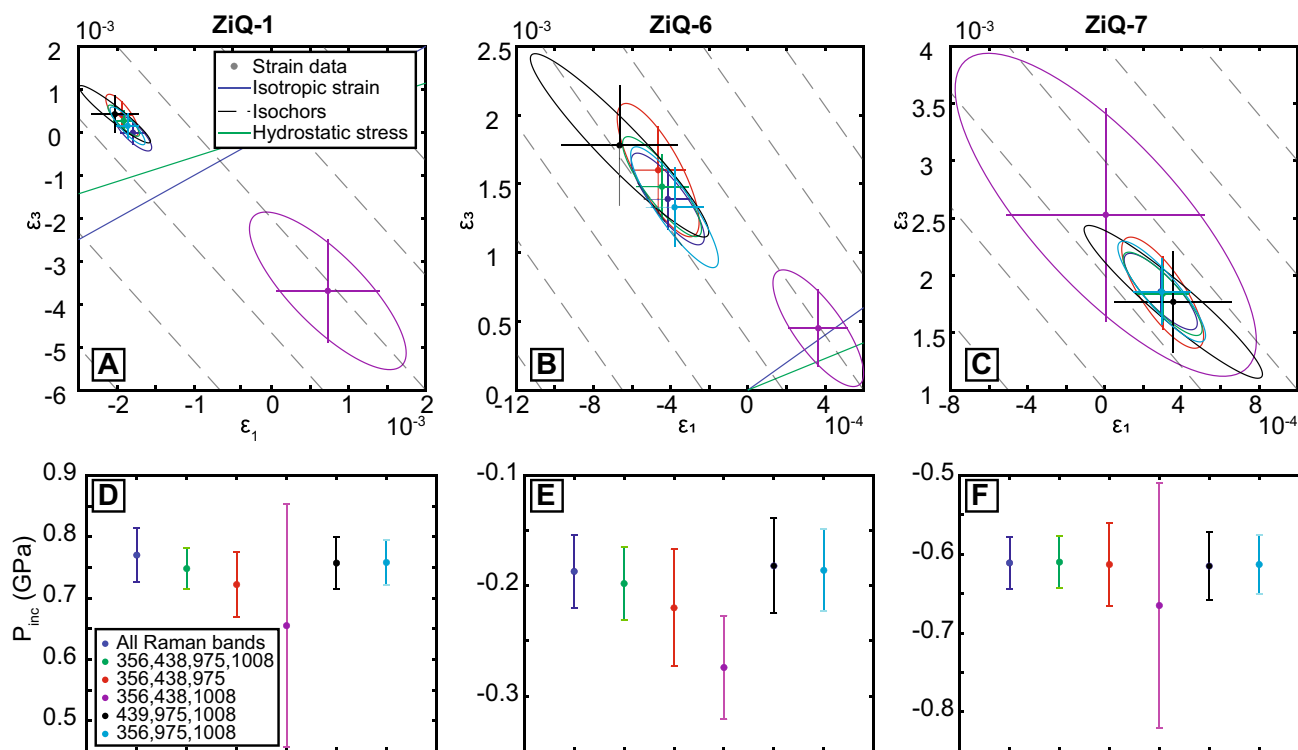
Fig. 3 Results of strain calculation tests for select inclusions from experiments ZiQ-1 (1 GPa, 900 °C), ZiQ-6 (1.5 GPa, 900 °C), and ZiQ-7 (2.0 GPa, 900 °C) using various combinations of Raman bands. The specific inclusions used for these tests are indicated with a "*" in Supplementary Table 1. **A–C** Plots of the calculated strains using the various combination of the Raman bands. Dashed lines are ZiQ isochors and the blue and green lines represent the lines of isotropic strain and hydrostatic stress. **D–F** Plots of the calculated P_{inc} for each of the strains calculated from various Raman band combinations shown in **A–C**

calculated from the zircon phonon-mode Grüneisen tensor. Data handling and plotting were performed using the EntraPT program (Mazzucchelli et al. 2021).

Calculation of expected inclusion strains and remnant pressure

The zircon inclusion P_{inc} values that were expected to develop upon exhumation from the experimental synthesis $P–T$ conditions to room conditions were calculated using both an isotropic elastic model (Angel et al. 2017b) and an anisotropic elastic model (Gonzalez et al. 2021). In the isotropic elastic model, the P_{inc} was calculated directly from the $P–T$ conditions of entrapment using the volume equations of state of quartz (Angel et al. 2017a) and zircon (Ehlers et al. 2021). This model uses isotropic elastic interaction and does not account for the host and inclusion elastic anisotropies or RCO.

In the anisotropic elastic model, the strains in the inclusion were calculated using the axial equations of state for quartz (Alvaro et al., 2020) and zircon (Ehlers et al. 2021) in the approach of Angel et al. (2021) that describes the unit-cell-parameter and the volume variations with pressure and temperature in a self-consistent manner. Mutual elastic interaction was accounted for using the elastic relaxation tensor (Mazzucchelli et al. 2019; Morganti et al. 2020) which depends on the RCO of the host and inclusion phases. However, the full three-dimensional orientations of each zircon inclusion in quartz are difficult to determine, so the individual RCOs of each zircon inclusion in quartz are not known. Therefore, we calculated the zircon-in-quartz relaxation tensor using the identity-RCO (i.e., in which the crystallographic c-axes of the quartz and zircon are aligned). This relaxation tensor was then applied to the strains obtained from the calculations with the axial-EoS to calculate the final elastic residual strains. The expected remnant pressures were calculated using the residual strains from the anisotropic model in conjunction with the elastic stiffness tensor of zircon (Özkan et al. 1974).

Results

Experimental synthesis and Raman measurements

All experiments over the range of 0.8–2.5 GPa and 700–900 °C crystallized zircon-in-quartz host–inclusion pairs. The size of crystallized quartz ranged from 100 to 1000 μm in maximum dimension and contained abundant zircon inclusions that are < 5 μm in maximum dimension (Fig. 2). The lowest temperature synthesis at 1.5 GPa and 700 °C crystallized abundant sub-μm zircon inclusions

that were too small to be reliably measured via Raman spectroscopy.

Measured Raman shifts from zircon inclusions in quartz are strongly affected by the inclusion geometry and lack of elastic isolation (Fig. 2; Mazzucchelli et al. 2018; Zhong et al. 2020a). Further, stiff inclusions contained in soft hosts undergo greater strain modifications due to geometry and lack of elastic isolation (see as an example the case of diamond-in-pyrope of Mazzucchelli et al. 2018). Therefore, we only measured the Raman spectra of elastically isolated inclusions that are > 5 inclusion radii from other inclusions and surfaces, and appeared relatively spherical. Raman spectra from zircon inclusions generally have well-defined peaks that display positive wavenumber shifts for low-pressure syntheses and negative wavenumber shifts for high-pressure syntheses (Fig. S2). Raman wavenumber shifts were used in hydrostatic pressure calibrations to estimate P_{inc} of the zircon inclusions (Binvignat et al. 2018; Schmidt et al. 2013). However, pressure values determined from the hydrostatic calibrations applied to different Raman bands in the same inclusion do not agree, suggesting that hydrostatic pressure calibrations of Raman band shifts with pressure cannot be used to determine P_{inc}.

Expected inclusion strain and remnant pressure

The expected strains and P_{inc} values that develop in a zircon inclusion entrapped in quartz during exhumation from the experimental conditions to room $P–T$ conditions were calculated using the anisotropic elastic model (Gonzalez et al. 2021). Angel et al., (2015) showed that the entrapment isomeke divides the $P–T$ space in two fields (Fig. 1). When the host–inclusion system deviates from the isomeke, the inclusion develops a compressive (positive) or tensile (negative) residual pressure (P_{inc}) depending on the contrast in elastic properties with its host. Figure 1 shows that for the ZiQ host–inclusion system, the fields of tensile and compressive strain and stress are inverted with respect to a typical soft-in-stiff host–inclusion system (Fig. 1A, B). Residual pressures of ZiQ inclusions are more compressive for an entrapment at low pressure or high temperature (Fig. 1C), but become tensile with increasing entrapment pressure or decreasing entrapment temperature (Fig. 1D). Expected P_{inc} values from the anisotropic model range from − 1.04 to 1.10 GPa (Table 1) and the expected P_{inc} values from the isotropic model are very similar and range from − 0.97 to 1.09 GPa. The expected values from the anisotropic model are used for comparison with the measured values because these values are the most accurate for this fully anisotropic host–inclusion system. Furthermore, from the anisotropic model results we can directly compare the measured inclusions strains with the expected strains as opposed to just the P_{inc} values.

Table 1 Experimental conditions with expected and measured P_{inc} results and discrepancies

Experimental parameters				Expected P_{inc}		Avg. measured P_{inc}		P_{inc} discrepancy[c]
				Isotropic	Anisotropic	Anisotropic		
Label	P (GPa)	T (°C)	# measured strained inclusions	P_{inc} iso (GPa)	P_{inc} (c_{ij}) (GPa)	P_{inc} (c_{ij}) (GPa)	Std	
Changing temperature								
ZiQ-6	1.5	900	37	0.15	0.11	−0.22	0.06	0.34
ZiQ-5	1.5	850	24	−0.06	−0.09	−0.40	0.10	0.31
ZiQ-11	1.5	800	31	−0.21	−0.25	−0.45	0.08	0.20
ZiQ-12	1.5	750	31	−0.33	−0.38	−0.53	0.13	0.16
ZiQ-13[a]	1.5	700	0	−0.44	−0.49	−	−	−
Changing pressure								
ZiQ-9[b]	0.8	900	33	1.09	1.10	0.74	0.12	0.36
ZiQ-1[b]	1	900	49	1.01	1.02	0.77	0.08	0.25
ZiQ-6	1.5	900	37	0.15	0.11	−0.22	0.06	0.34
ZiQ-7	2	900	33	−0.49	−0.55	−0.59	0.16	0.04
ZiQ-10	2.2	900	2	−0.69	−0.76	−0.90	0.12	0.14
ZiQ-8[a]	2.5	900	0	−0.97	−1.04	−	−	−
QTiP measurements								
QTiP44a	1	925	34	1	1	0.5	0.12	0.5
QTiP38	0.5	800	7	1.26	1.29	0.85	0.31	0.46

'Std' is the 1σ standard deviation of the P_{inc} values

[a] All Raman shifts are indistinguishable from peak position of reference material

[b] Experiment performed in the β-quartz stability field

[c] Indicates the $abs(P_{inc\,aniso,c_{ij}}^{expect} - P_{inc\,c_{ij}}^{meas})$

## Remnant strains in synthesized inclusions and elastic calculations

Strains from measured inclusions plot in clusters elongated parallel to isochors (Fig. 4B, C). However, the measured strains are not within error of the expected residual strains calculated with the elastic model for the experimental entrapment conditions. Instead, the measured strains plot on an isochor to the right of the expected isochor. We calculated the residual pressure from the measured strains with the elastic stiffness tensor of zircon (Özkan et al. 1974). Figure 4D shows that the P_{inc} measured in the inclusions are always more tensile than the P_{inc} values expected from purely elastic calculations. In detail, experiments that were anticipated to give large compressive P_{inc} values yielded lower P_{inc} values (e.g., ZiQ-1, 9), while experiments that were anticipated to give tensile P_{inc} yielded greater magnitude tensile P_{inc} values (e.g., ZiQ-5, 11, 12). One experiment (ZiQ-6) was anticipated to give a compressive P_{inc} but the measured P_{inc} values are tensile (Fig. 5). These measured P_{inc} values were then used to calculate entrapment isomekes of the synthesized inclusions for comparison with the experimental P–T conditions. P_{inc} values are normally distributed (Fig. 5) and were averaged and used to calculate a single isomeke. Since the measured P_{inc} values are more tensile than the expected

values, the calculated entrapment isomekes plot to the left of the expected isomekes. Therefore, the isomekes from the measurements overestimate the entrapment pressure with respect to the experimental pressure and underestimate the entrapment temperature with respect to the experimental temperature (Fig. 6A).

Discussion

Potential reasons for observed discrepancies

Our experimental results and calculations show that zircon inclusions entrapped in quartz hosts retain remnant strains that can be used to determine inclusion pressures. Comparing the measured and expected strains and P_{inc} values, we see that the trends are consistent and correct but the magnitudes are systematically more tensile (Fig. 4D). Previous experiments (e.g., Thomas and Spear 2018; Bonazzi et al. 2019; Pummel 2021), assessment of mineral and phase boundaries (Osborne et al. 2019), and consistency between thermobarometry results evaluated with different methods (e.g., Zr-in-rutile data in Tomkins et al. 2007; Thomas et al. 2015; Osborne et al. 2022) suggest that the piston cylinders are accurately calibrated over the P–T range of quartz
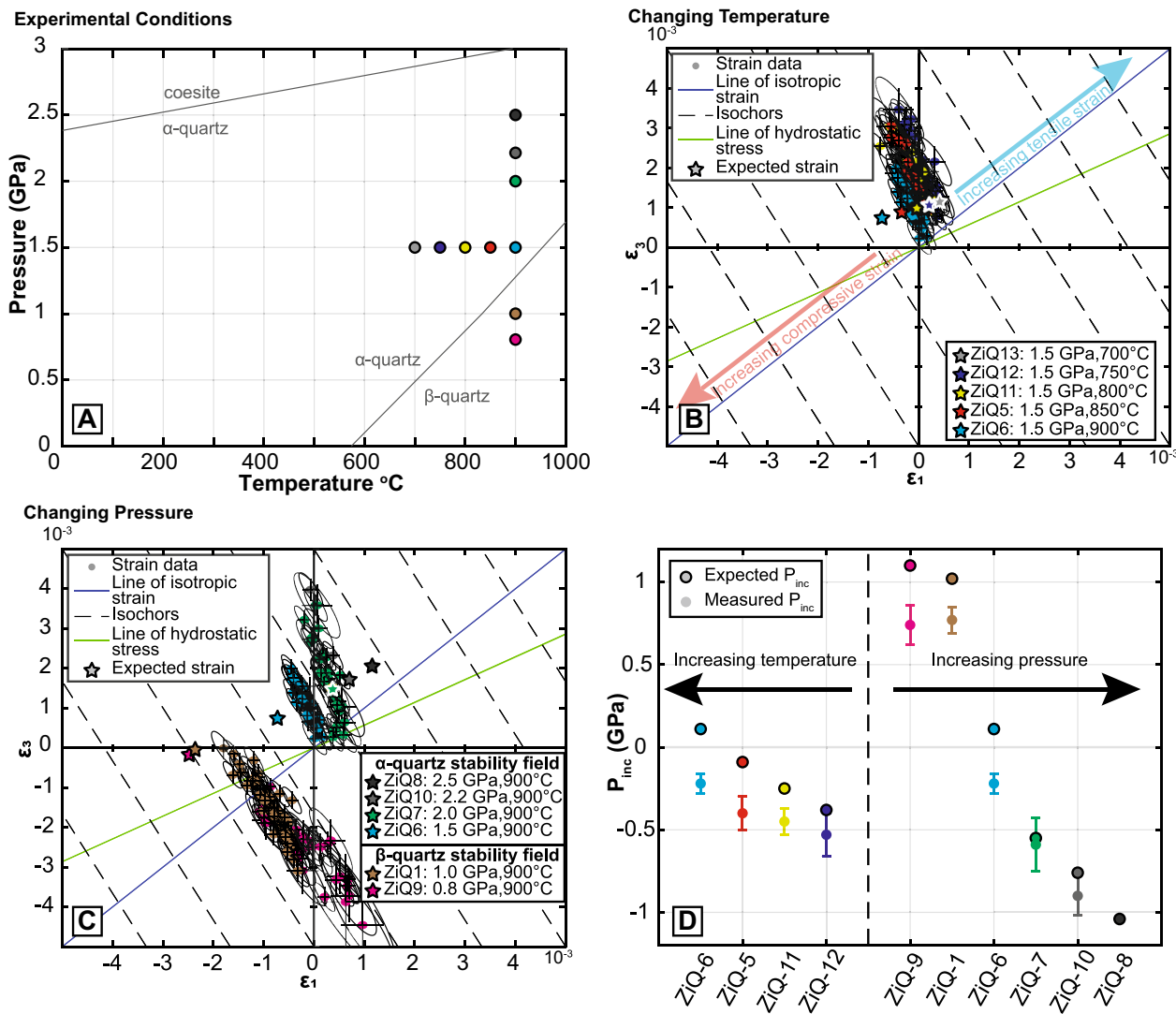
Fig. 4 Experimental conditions and results. **A** *P–T* diagram of the experimental conditions. **B–C** Plots of the measured and expected ε_1 and ε_3 strains divided into changing temperature at 1.5 GPa (**B**) and changing pressure at 900 °C (**C**). The larger bold stars represent the expected residual strains. Dashed lines are ZiQ isochors and the blue and green lines represent the lines of isotropic strain and hydrostatic stress. **D** Plot comparing the measured average P_{inc} and the expected P_{inc} divided into the changing temperature and changing pressure experiments. The error bars are the 1σ standard deviation of the measured P_{inc} values

stability. Here, we evaluate the potential effects of analytical biases and the assumptions of the elastic calculations on the measured ZiQ strains and P_{inc} values.

Isotropic elasticity assumptions and the Grüneisen tensor

Two elastically anisotropic inclusions entrapped in an anisotropic host mineral at the same *P–T* conditions but with different orientations will be subject to different strain states that can break their crystallographic symmetry (Gonzalez et al. 2021; Murri et al. 2022). Irregular geometries of inclusions will further modify the strain

state of the inclusions from that of an ideal spherical inclusion (Mazzucchelli et al. 2018; Campomenosi et al. 2018; Zhong et al. 2020a). In this study, the identity-RCO and a spherical geometry were used for the calculation of zircon-in-quartz strains. However, Fig. 2 shows that both of these assumptions are violated and may never be truly met in real inclusions. The distributions of P_{inc} are systematically more negative than the expected P_{inc} values from both elastic models (Fig. 5). We expect that, if both inclusion RCO and geometry are random, then the distribution of measured inclusion P_{inc} would still overlap with the expected P_{inc} values because some of

Increasing temperature ➞

Increasing pressure ➞
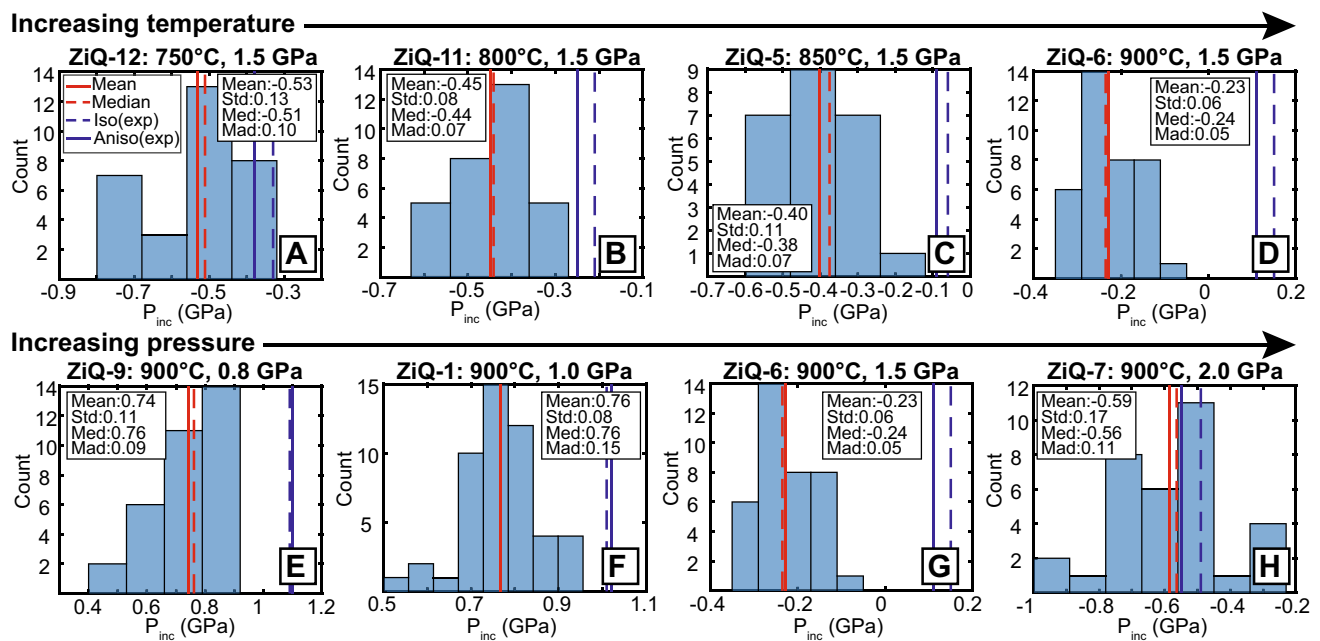
Fig. 5 Plots of the individual P_{inc} calculated from the Raman measurements, with means and mediums indicated by the red vertical lines, compared to the expected (exp) P_{inc} values (blue lines). ZiQ-8 and 10 were not plotted because the inclusions do not preserve remnant pressures. 'Std' is the 1σ standard deviation and 'Mad' is the median absolute deviation

the inclusions would be closer to the assumed geometry and RCO. Instead, the systematically more tensile P_{inc} distributions of the measured inclusions argues that the observed discrepancies cannot be attributed solely to inclusion geometry or RCO.

The zircon phonon-mode Grüneisen tensor is believed to be accurate because it accurately reproduces the room-temperature pressure dependency of the zircon Raman bands (Stangarone et al. 2019). However, the sensitivity of the zircon phonon-mode Grüneisen tensor to symmetry-breaking strains is not well constrained. The effects of symmetry breaking on the quartz phonon-mode Grüneisen tensor were recently evaluated using DFT simulations of a quartz inclusion in a zircon host at conditions along the quartz–coesite phase boundary (Murri et al. 2022). Despite this entrapment pressure at the practical limits of the quartz stability field, the discrepancies in P_{inc} and entrapment pressures between the symmetry broken strains and those from the Grüneisen tensor are relatively small. In the ZiQ system, the effect of symmetry breaking should be smaller because the stiff zircon will develop less strain and therefore undergo less symmetry breaking during decompression and cooling to room conditions. Therefore, we anticipate that the effects of symmetry breaking on the strains calculated using the zircon phonon-mode Grüneisen tensor are also relatively small and unlikely to produce the observed discrepancies.

Potential local perturbations of inclusion strains

The measured inclusion strains and P_{inc} can be modified by localized effects around zircon inclusions including the proximity of inclusions to grain boundaries or inhomogeneities (Campomenosi et al. 2018) and potential multi-phase behavior (Musiyachenko et al. 2021). The proximity of the inclusion to the host grain boundaries will reduce the magnitude of the inclusion pressures toward ambient pressure and, even when purely elastic, relax the residual pressure to less than the P_{inc} predicted by an elastic model of an isolated inclusion (Campomenosi et al. 2018). In the case of the ZiQ host–inclusion system, relaxation of a tensile P_{inc} toward ambient conditions reduces the calculated entrapment pressure at a given entrapment temperature, and the relaxation of a compressive P_{inc} increases the entrapment pressure (Fig. 7). However, modification of P_{inc} due to relaxation induced by proximity to host grain boundaries or inhomogeneities cannot cause the compressive stress of an inclusion to become tensile or vice versa. Therefore, this mechanism is inconsistent with the results of experiment ZiQ-6 which has positive expected P_{inc} values, but the measured inclusion P_{inc} values are tensile. Furthermore, experiments ZiQ-5 and ZiQ-11 are also inconsistent with relaxation toward ambient conditions because both have negative expected P_{inc} values but the measured inclusions yield greater magnitude tensile P_{inc} values.
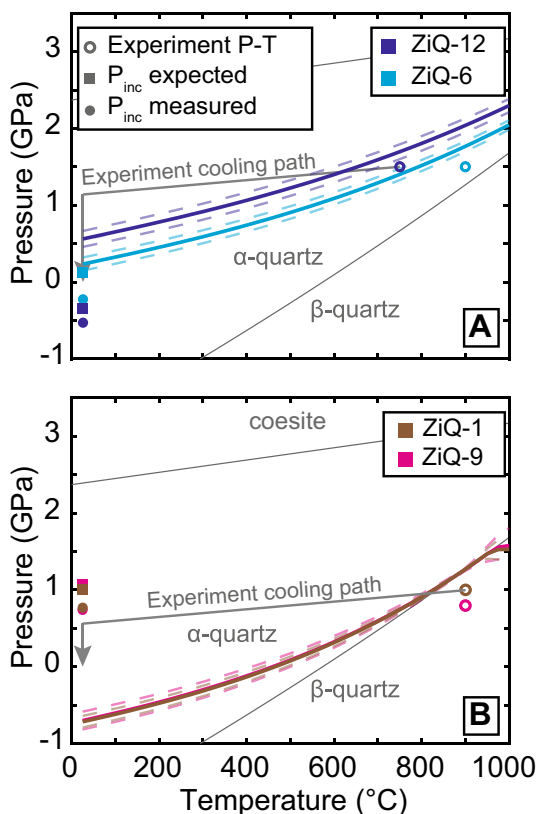
Fig. 6 Calculated apparent entrapment isomekes. **A** Calculated entrapment isomekes and P_{inc} of α-quartz experiments. **B** Calculated entrapment isomekes and P_{inc} of β-quartz experiments. The dashed lines on the isomekes indicate the range of P_{trap} values corresponding to the 1σ standard deviation of the P_{inc} values. α-quartz–coesite phase boundary from Osborne et al. (2019), α–β quartz room P–T phase boundary from Angel et al. (2017a)

In the application of elastic thermobarometry, it is assumed that the host and inclusion are the only phases present in the system and that both are compositionally homogeneous. In practice, however, mineral inclusions or their host can consist of multiple phases or contain fluids (e.g., Musiyachenko et al. 2021; Angel et al. 2023). No other minerals formed in our experiments because all experiments were performed within the stability field of quartz and zircon with a starting mixture of SiO_2, ZrO_2 and H_2O. However, it is possible that aqueous fluids were incorporated into zircon inclusions and altered the measured P_{inc} values. The potential effect of fluids in zircon inclusions on P_{inc} was evaluated using EoSFit7c (Angel et al. 2023). When small amounts of water ($< 10\%$ of the total cavity volume) are present in the inclusion the P_{inc} will be shifted toward zero pressure. This trend is inconsistent with the results of multiple experiments where the measured P_{inc} values are larger in magnitude than the expected values. Additionally, the Raman spectra of our measured zircon inclusions lack the characteristic bands of water at 3600 and 3460 cm^{-1}.

Non-elastic deformation of ZiQ host–inclusion systems

Distributions of P_{inc} that are systematically more tensile than the expected P_{inc} values cannot be attributed to the analytical biases or assumptions of the elastic calculations. These conclusions combined with the fact that the trends of measured and expected strains and P_{inc} are consistent and correct suggests that the host and inclusion EoS and the experimental approach are correct. Therefore, the observed discrepancies must be ascribed to additional complexities that affected the
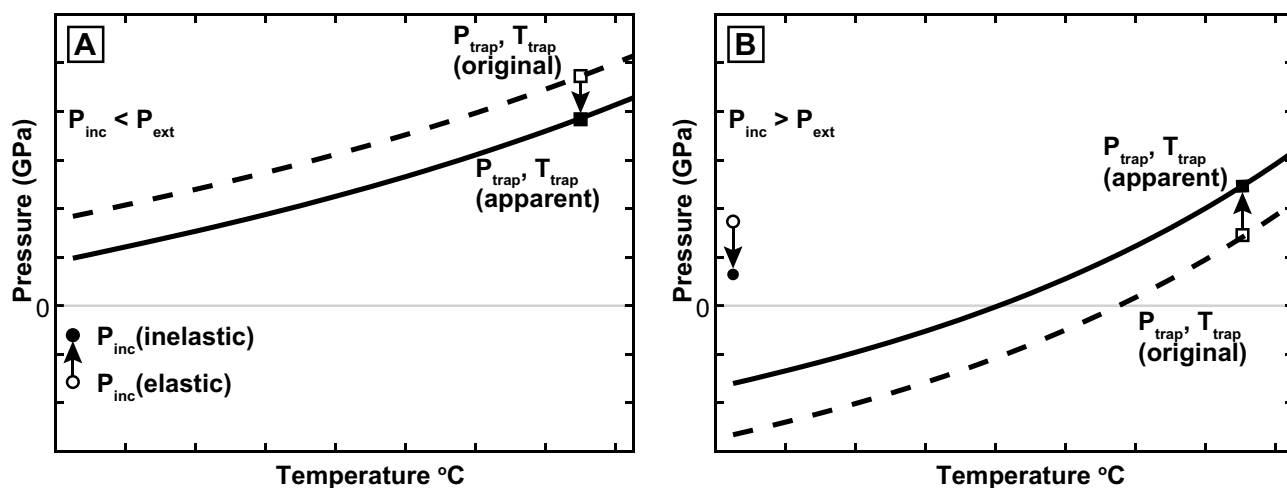
Fig. 7 Schematic diagrams illustrating the effect of partial inelastic relaxation of a tensile (negative) P_{inc} and compressive (positive) P_{inc} on the calculated ZiQ entrapment isomekes and the inferred entrapment conditions. P_{trap}(original) is the inclusion entrapment conditions determined from the original P_{inc} (elastic) value.

determined from the original P_{inc} (elastic) value. P_{trap} (apparent) is the calculated inclusion entrapment condition determined from P_{inc} (inelastic) which has been inelastically relaxed by localized effects around the inclusion

host–inclusion pairs during synthesis or experimental cooling and decompression.

Inelastic deformation during cooling in the α-quartz field

Several trends that give insight into the deformational behavior of zircon inclusions in quartz become apparent when the experimental results are divided into those performed in the stability fields of the α and β phases of quartz. For the experiments performed in the α-quartz stability field at the same pressure with different temperatures (Fig. 4A), the largest discrepancy between the expected and measured P_{inc} occurs for the highest temperature experiment at 1.5 GPa and 900 °C (ZiQ-6, Fig. 4C). This discrepancy decreases with decreasing experimental temperature and is smallest for the lowest temperature experiment at 750 °C (ZiQ-12). For the experiments performed at the same temperature but different pressures in the α-quartz field (i.e., ZiQ-6, 7, 10) the measured P_{inc} values are similarly more tensile than those expected from the elastic model. However, in this group of experiments, we found that a majority or all of the inclusions in the two highest-pressure experiments (ZiQ-10, ZiQ-8) yield $P_{inc} \approx 0$ implying complete inelastic relaxation of these inclusions.

These observations are all consistent with partial inelastic relaxation of the inclusion strains due to viscous and/or plastic deformation during the experimental cooling and decompression (Fig. 6). Evaluation of the stress state of a zircon inclusion entrapped in an α-quartz host along the "exhumation" or recovery P–T path in our experiments shows that P_{inc} initially increases due to the elastic response of a stiff-in-soft host–inclusion system being brought into the stress field above the entrapment isomeke during cooling (Fig. 1C, D). Along this path, the large stresses that develop in the inclusions can then induce inelastic deformation of the host quartz. This relaxation will decrease the magnitude of the P_{inc} toward the external pressure (Zhong et al. 2020b). Once the temperature along the path is sufficiently low, the inelastic relaxation becomes negligible, and the deformation is purely elastic for the remaining part of the path to room conditions. The consequences for a stiff inclusion in a soft host are (1) the measured P_{inc} values are more tensile than the expected values calculated using a purely elastic model, and (2) the calculated "apparent" entrapment isomekes plot at lower temperatures than the true entrapment isomekes (i.e., to the left, Fig. 6A). The magnitude of the relaxation depends on the characteristics of the path (i.e., the P–T of entrapment, and the cooling rate; Zhong et al. 2020b), such that experiments performed at lower temperatures undergo less inelastic relaxation. This explains why the lowest temperature experiment (ZiQ-12) yields the smallest discrepancies between the measured and expected P_{inc} values and entrapment conditions (Figs. 4D, 6A). Furthermore, the

inclusions in the highest-pressure experiments (ZiQ-10 and ZiQ-8) are expected to have extremely tensile P_{inc} values (<-1 GPa). However, these large tensile stresses can induce large differential stresses in the host quartz and produce a complete inelastic relaxation of the inclusion stress (e.g., Campomenosi et al. 2023), explaining the complete relaxation of the P_{inc} values of the inclusions in these experiments.

## Inelastic deformation at the α–β quartz transition

Zircon inclusions from the β-quartz syntheses yield measured ε_1 strains that are much more tensile than the expected ε_1 strains and therefore give positive P_{inc} values that are less compressive than the expected values (Fig. 4C). When the measured P_{inc} values are used to calculate entrapment isomekes, the apparent isomekes for both experiments overlap very closely with the α–β quartz phase boundary (Fig. 6B). This suggests that ZiQ host–inclusion systems reset inelastically when crossing the phase transition from β- to α-quartz because the bulk modulus of quartz approaches zero at the phase transition (Lakshtanov et al. 2007), which facilitates the plastic deformation of the quartz host. However, once the transition is crossed, the bulk modulus rebounds, resulting in the re-stiffening of the quartz (e.g., Angel et al. 2017a). This behavior explains why these measured inclusion strains give fundamentally different discrepancies from the syntheses in the α-quartz field and also do not return the experimental synthesis P–T conditions. However, these results also imply that zircon inclusions originally entrapped in β-quartz can be used to determine the P–T conditions at which the host–inclusion system crossed the phase transition boundary.

If this analysis is correct, we expect that this behavior should occur for all inclusions hosted by β-quartz regardless of their entrapment P–T or mineralogy. Therefore, we confirmed this result by performing additional measurements of zircon inclusions entrapped in β-quartz that were synthesized during the Ti-in-quartz calibration experiments of Thomas et al. (2010) and Osborne et al. (2022). Following the same approach described for the ZiQ experiments, we found that the ε_1 strains for these inclusions are similarly more tensile than the expected ε_1 strains (Fig. 8a) and their entrapment isomekes also plot along the phase transition line (Fig. 8b).
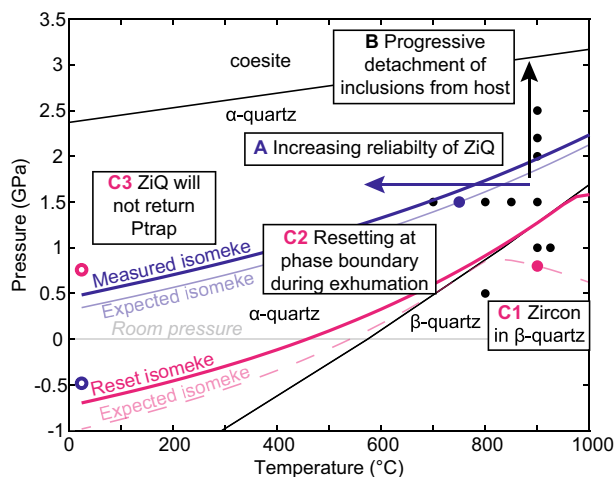
Conclusions

Evaluation of the behavior of stiff zircon inclusions contained in soft quartz host crystals shows that the interpretation of their inclusion pressures is complicated due to the rheology of quartz and its α–β phase transition. Interpreting our results in the framework of the physical behavior of quartz in P–T space reveals three processes that affect the
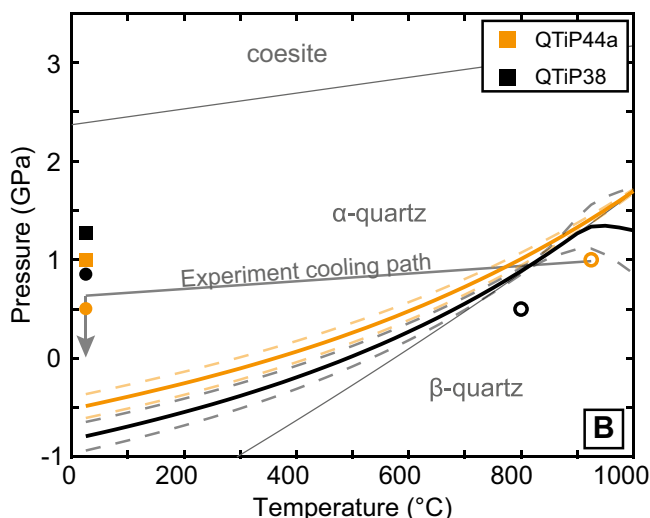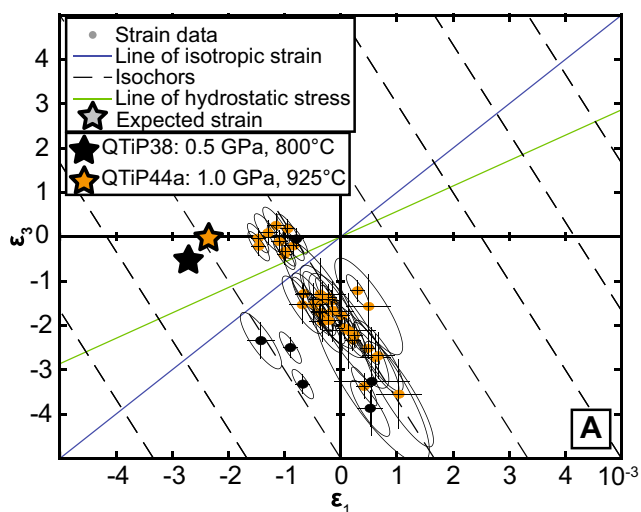
Fig. 8 Results from additional measurements of experimental samples. **A** Measured residual strains in zircon inclusions in quartz from Ti-in-Quartz experiments determined using Raman spectroscopy and the zircon phonon-mode Grüneisen tensor. The larger bold circles represent the residual strains expected from elastic calculations. Dashed lines are isochors for a zircon inclusion in quartz and the solid blue and green lines represent the lines of isotropic strain and hydrostatic stress, respectively. **B** Calculated isomekes and P_{inc} values. Squares represent the expected P_{inc} values and the circles are the measured values. Open circles indicate the experimental run conditions

Fig. 9 Guide to interpreting the strain and P_{inc} of ZiQ. Solid circles indicate the ZiQ synthesis P–T conditions and the P–T of the experiments from Thomas et al. (2010) and Osborne et al. (2022). **A** For zircon inclusions entrapped in α-quartz, entrapment pressures calculated using measured P_{inc} values are more accurate at lower temperatures. **B** Zircon inclusions entrapped in quartz at high-pressure are subject to large tensile strains and will progressively detach from the quartz host. **C** Zircon inclusions entrapped in β-quartz will be reset as the host–inclusion system crosses the α–β quartz phase boundary and calculated isomekes will not return the P–T of entrapment

strains and stresses preserved in synthesized zircon inclusions hosted in quartz (Fig. 9):

1. plastic resetting of the P_{inc} of zircon in α-quartz at high temperatures after entrapment resulting in more tensile

P_{inc} values and corresponding isomekes that plot to the left of true entrapment isomekes. These are more reliable for the estimation of entrapment conditions at relatively low temperatures where temperature-dependent inelastic relaxation is less.
2. large tensile strain states of zircon inclusions in quartz may lead to partial or complete relaxation of the P_{inc}, so that zircon inclusions with $P_{inc} = 0$ may have been entrapped at higher pressures than those calculated with an elastic model using a $P_{inc} = 0$.
3. inclusions entrapped in β-quartz mechanically reset at the α–β phase transition.

This last result implies that inclusions entrapped in β-quartz will not record the conditions of entrapment but instead can potentially be used to constrain the P–T conditions at which the exhumation path crossed the phase boundary. However, since inclusions exhumed from the β-quartz field will still be subject to the processes that occur in the α-quartz field, it is possible that only host–inclusion systems that crossed the phase boundary at sufficiently low P–T conditions will record the conditions of the exhumation path and the phase boundary.

We anticipate that this host–inclusion system could be particularly useful for obtaining P–T constraints on the exhumation path of rapidly exhumed high-temperature metamorphic and igneous rocks, such as felsic volcanic systems. For example, zircon-in-quartz thermobarometric constraints could be coupled with well-established thermobarometric methods, such as Ti-in-quartz thermobarometry (Thomas

et al. 2010), Ti-in-zircon thermometry (Ferry and Watson 2007), or zircon saturation thermometry (Watson and Harrison 1983; Crisp and Berry 2022) to gain detailed insight into volcanic processes. However, future applications of zircon-in-quartz to natural rocks must also carefully evaluate the radiation damage of zircon inclusions, which can be significant and affect calculated elastic equilibrium P–T conditions (e.g., Campomenosi et al. 2020).

Since the complexities of the zircon-in-quartz host–inclusion system are not linked to the elasticity of stiff-in-soft host–inclusion systems, but rather the rheological behavior of quartz, we conclude that stiff inclusions contained in soft host minerals can be used for Raman thermobarometry. However, caution must be paid to inelastic effects, which may be significant depending on the rheology of the host and conditions of entrapment.

Data availability All data is provided in the supplementary tables.

References

Alvaro M, Mazzucchelli ML, Angel RJ, Murri M, Campomenosi N, Scambelluri M, Nestola F, Korsakov A, Tomilenko AA, Marone F, Morana M (2020) Fossil subduction recorded by quartz from the coesite stability field. Geology 48(1):24–28. https://doi.org/10.1130/G46617.1

Angel RJ, Mazzucchelli ML, Alvaro M, Nimis P, Nestola F (2014) Geobarometry from host-inclusion systems: the role of elastic relaxation. Am Mineral 99(10):2146–2149. https://doi.org/10.2138/am-2014-5047

Angel RJ, Nimis P, Mazzucchelli ML, Alvaro M, Nestola F (2015) How large are departures from lithostatic pressure? Constraints from host-inclusion elasticity. J Metamorph Geol 33(8):801–813. https://doi.org/10.1111/jmg.12138

Angel RJ, Alvaro M, Miletich R, Nestola F (2017a) A simple and generalized P-T–V EoS for continuous phase transitions, implemented in EosFit and applied to quartz. Contrib Miner Petrol 172(5):1–15. https://doi.org/10.1007/s00410-017-1349-x

Angel RJ, Mazzucchelli ML, Alvaro M, Nestola F (2017b) EosFit-Pinc: a simple GUI for host-inclusion elastic thermobarometry. Am Mineral 102(9):1957–1960. https://doi.org/10.2138/am-2017-6190

Angel RJ, Murri M, Mihailova B, Alvaro M (2019) Stress, strain and Raman shifts. Z Kristallogr 234(2):129–140. https://doi.org/10.1515/zkri-2018-2112

Angel R, Mazzucchelli M, Gonzalez-platas J, Alvaro M (2021) A self-consistent approach to describe unit-cell- parameter and volume variations with pressure and temperature research papers. J Appl Crystallogr 54:1621–1630. https://doi.org/10.1107/S1600576721009092

Angel RJ, Mazzucchelli ML, Musiyachenko KA, Nestola F, Alvaro M (2023) Elasticity of mixtures and implications for piezobarometry of mixed-phase inclusions. Eur J Mineral 35:461–478 (**in press**)

Baldwin SL, Schönig J, Gonzalez JP, Davies H, Eynatten HV (2021) Garnet sand reveals rock recycling processes in the youngest exhumed high- and ultrahigh-pressure terrane on Earth. Proc Natl Acad Sci USA 118(3):1–8. https://doi.org/10.1073/pnas.2017231118

Binvignat FAP, Malcherek T, Angel RJ, Paulmann C, Schlüter J, Mihailova B (2018) Radiation-damaged zircon under high pressures. Phys Chem Miner 45(10):981–993. https://doi.org/10.1007/s00269-018-0978-6

Bonazzi M, Tumiati S, Thomas JB, Angel RJ, Alvaro M (2019) Assessment of the reliability of elastic geobarometry with quartz inclusions. Lithos 350–351:105201. https://doi.org/10.1016/j.lithos.2019.105201

Boyd FR, England JL (1960) The quartz-coesite transition. J Geophys Res 65:749–756. https://doi.org/10.1029/JZ065i002p00749

Campomenosi N, Mazzucchelli ML, Mihailova BD, Scambelluri M, Angel RJ, Nestola F, Reali A, Alvaro M (2018) How geometry and anisotropy affect residual strain in host inclusion system: coupling experimental and numerical approaches. Am Mineral 103(12):2032–2035. https://doi.org/10.1111/ijlh.12426

Campomenosi N, Rubatto D, Hermann J, Mihailova B, Scambelluri M, Alvaro M (2020) Establishing a protocol for the selection of zircon inclusions in garnet for Raman thermobarometry. Am Mineral 105(July):992–1001. https://doi.org/10.2138/am-2020-7246

Campomenosi N, Angel RJ, Alvaro M, Mihailova B (2023) Resetting of zircon inclusions in garnet: implications for elastic thermobarometry. Geology 51(1):23–27. https://doi.org/10.1130/G50431.1/5733973/g50431.pdf

Crisp LJ, Berry AJ (2022) A new model for zircon saturation in silicate melts. Contrib Mineral Petrol 177(7):1–24. https://doi.org/10.1007/s00410-022-01925-6

Ehlers AM, Zaffiro G, Angel RJ, Boff-Ballaran T, Carpenter MA, Alvaro M, Ross NL (2022) Thermoelastic properties of zircon: implications for geothermobarometry. Am Mineral 107(1):74–81. https://doi.org/10.2138/am-2021-7731

Ferry JM, Watson EB (2007) New thermodynamic models and revised calibrations for the Ti-in-zircon and Zr-in-rutile thermometers. Contrib Mineral Petrol 154(4):429–437. https://doi.org/10.1007/s00410-007-0201-0

Gilio M, Scambelluri M, Angel RJ, Alvaro M (2021) The contribution of elastic geothermobarometry to the debate on HP vs. UHP

metamorphism. J Metamorph Geol 40(2):229–242. https://doi.org/10.1111/jmg.12625

Gonzalez JP, Thomas JB, Baldwin SL, Alvaro M (2019) Quartz-in-garnet and Ti-in-quartz thermobarometry: methodology and first application to a quartzofeldspathic gneiss from eastern Papua New Guinea. J Metamorph Geol 37:1193–1208. https://doi.org/10.1111/jmg.12508

Gonzalez JP, Mazzucchelli ML, Angel RJ, Alvaro M (2021) Elastic geobarometry for anisotropic inclusions in anisotropic host minerals: quartz-in-zircon. J Geophys Res Solid Earth. https://doi.org/10.1029/2021JB022080

Guiraud M, Powell R (2006) P-V-T relationships and mineral equilibria in inclusions in minerals. Earth Planet Sci Lett 244(3–4):683–694. https://doi.org/10.1016/j.epsl.2006.02.021

Kohn MJ (2014) "Thermoba-Raman-try": calibration of spectroscopic barometers and thermometers for mineral inclusions. Earth Planet Sci Lett 388:187–196. https://doi.org/10.1016/j.epsl.2013.11.054

Kohn MJ, Mazzucchelli ML, Alvaro M (2023) Elastic thermobarometry. Annu Rev Earth Planet Sci 51:331–366

Lakshtanov DL, Sinogeikin SV, Bass JD (2007) High-temperature phase transitions and elasticity of silica polymorphs. Phys Chem Miner 34(1):11–22. https://doi.org/10.1007/s00269-006-0113-y

Mazzucchelli ML, Burnley P, Angel RJ, Morganti S, Domeneghetti MC, Nestola F, Alvaro M (2018) Elastic geothermobarometry: corrections for the geometry of the host-inclusion system. Geology 46(3):231–234. https://doi.org/10.1130/G39807.1

Mazzucchelli ML, Reali A, Morganti S, Angel RJ, Alvaro M (2019) Elastic geobarometry for anisotropic inclusions in cubic hosts. Lithos 350–351:105218. https://doi.org/10.1016/j.lithos.2019.105218

Mazzucchelli ML, Angel RJ, Alvaro M (2021) EntraPT: an online platform for elastic geothermobarometry. Am Mineral 106(5):830–837. https://doi.org/10.2138/am-2021-7693ccbyncnd

Morganti S, Mazzucchelli ML, Alvaro M, Reali A (2020) A numerical application of the Eshelby theory for geobarometry of non-ideal host-inclusion systems. Meccanica 55(4):751–764. https://doi.org/10.1007/s11012-020-01135-z

Murri M, Gonzalez JP, Mazzucchelli ML, Prencipe M, Mihailova B, Angel RJ, Alvaro M (2022) The role of symmetry-breaking strains on quartz inclusions in anisotropic hosts: implications for Raman elastic geobarometry. Lithos 422–423(April):106716. https://doi.org/10.1016/j.lithos.2022.106716

Musiyachenko KA, Murri M, Prencipe M, Angel RJ, Alvaro M (2021) A Grüneisen tensor for rutile and its application to host-inclusion systems. Am Mineral 106(August):1586–1595. https://doi.org/10.2138/am-2021-7618

Osborne ZR, Thomas JB, Nachlas WO, Baldwin SL, Holycross ME, Spear FS, Watson EB (2019) An experimentally calibrated thermobarometric solubility model for titanium in coesite (TitaniC). Contrib Mineral Petrol 175:1–13. https://doi.org/10.1007/s00410-019-1575-5

Osborne ZR, Thomas JB, Nachlas WO, Angel RJ, Hoff CM, Watson EB (2022) TitaniQ revisited: expanded and improved Ti-in-quartz solubility model for thermobarometry. Contrib Mineral Petrol 177(31):1–21. https://doi.org/10.1007/s00410-022-01896-8

Özkan H, Cartz L, Jamieson JC (1974) Elastic constants of non-metamict zirconium silicate. J Appl Phys 45(2):556–562. https://doi.org/10.1063/1.1663283

Pummel BA (2021) Experimental evaluation of stress relaxation of quartz inclusions in garnet. Master's of Science thesis, Syracuse University

Schmidt C, Steele-MacInnis M, Watenphul A, Wilke M (2013) Calibration of zircon as a Raman spectroscopic pressure sensor to high temperatures and application to water-silicate melt systems. Am Mineral 98(4):643–650. https://doi.org/10.2138/am.2013.4143

Stangarone C, Angel RJ, Prencipe M, Campomenosi N, Mihailova B, Alvaro M (2019) Measurement of strains in zircon inclusions by Raman spectroscopy. Eur J Mineral 31(4):685–694. https://doi.org/10.1127/ejm/2019/0031-2851

Thomas JB, Spear FS (2018) Experimental study of quartz inclusions in garnet at pressures up to 30 GPa: evaluating validity of the quartz-in-garnet inclusion elastic thermobarometer. Contrib Mineral Petrol 173(42):1–14. https://doi.org/10.1007/s00410-018-1469-y

Thomas JB, Watson EB, Spear FS, Shemella PT, Nayak SK, Lanzirotti A (2010) TitaniQ under pressure: the effect of pressure and temperature on the solubility of Ti in quartz. Contrib Mineral Petrol 160(5):743–759. https://doi.org/10.1007/s00410-010-0505-3

Thomas JB, Watson EB, Spear FS, Wark DA (2015) TitaniQ recrystallized: experimental confirmation of the original Ti-in-quartz calibrations. Contrib Mineral Petrol 169(27):1–16. https://doi.org/10.1007/s00410-015-1120-0

Tomkins HS, Powell R, Ellis DJ (2007) The pressure dependence of the zirconium-in-rutile thermometer. J Metamorph Geol 25(6):703–713. https://doi.org/10.1111/j.1525-1314.2007.00724.x

Watson EB, Harrison TM (1983) Zircon saturation revisited: temperature and composition effects in a variety of crustal magma types. Earth Planet Sci Lett 64(2):295–304. https://doi.org/10.1016/0012-821X(83)90211-X

Zhang Y (1998) Mechanical and phase equilibria in inclusion–host systems. Earth Planet Sci Lett 157:209–222. https://doi.org/10.1016/S0012-821X(98)00036-3

Zhong X, Dabrowski M, Jamtveit B (2020a) Analytical solution for residual stress and strain preserved in anisotropic inclusion entrapped in isotropic host. Solid Earth 12:817–833. https://doi.org/10.5194/se-2020-180

Zhong X, Moulas E, Tajčmanová L (2020b) Post-entrapment modification of residual inclusion pressure and its implications for Raman elastic thermobarometry. Solid Earth 11:223–240. https://doi.org/10.5194/se-11-223-2020